Supplemental Materials

AeroTrans: Hourly AOD Retrieval over Land from MSG-1/SEVIRI Imagery Integrating Transformer and Transfer Learning

Yulong Fan[1], Zhanqing Li[2*], Lin Sun[1*], Oleg Dubovik[3], Zhihui Wang[4], Fan Cheng[5], Xiaohang Shi[6], Jing Wei[7*]

1. College of Geodesy and Geomatics, Shandong University of Science and Technology, Qingdao, China
2. Department of Atmospheric and Oceanic Science, Earth System Science Interdisciplinary Center, University of Maryland, College Park, MD, USA
3. Laboratoire d'Optique Atmosphérique, Université de Lille, CNRS, Lille, France
4. University of Science and Technology of China, Hefei, China
5. School of Environmental and Sustainable Engineering, Eastern Institute of Technology Ningbo, Ningbo, China
6. State Key Laboratory of Climate System Prediction and Risk Management, School of Atmospheric Physics, Nanjing University of Information Science and Technology, Nanjing, China
7. MEEKL-AERM, College of Environmental Sciences and Engineering, Institute of Tibetan Plateau, and Center for Environment and Health, Peking University, Beijing, China

*Corresponding authors:

zhanqing@umd.edu; sunlin6@126.com; jingwei@pku.edu.cn

Contents

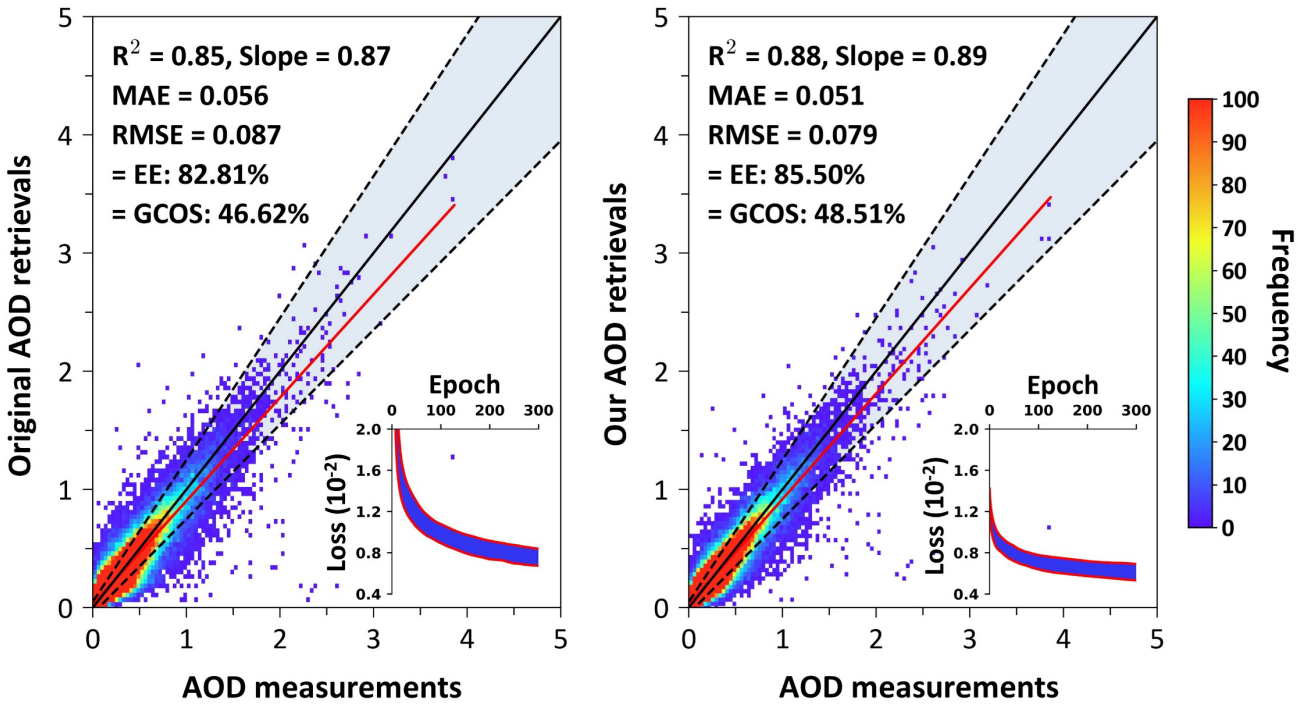

Figure S1. Density scatter plots of (a) original model (trained directly without pre-training) and (b) our model (pre-trained and fine-tuned) for hourly AOD retrievals against ground-based measurements, assessed using sample-based ten-fold cross-validation approaches. In each panel, the black dotted line represents the expected error range, the black solid line indicates the 1:1 line, the red solid line shows the linear regression line, and the subgraph illustrates the fluctuation of loss values (10^{-2}) over the training process. The numbers in the top-left corner of the subfigure represent the coefficient of determination (R^2), slope of the regression line, mean absolute error (MAE), root mean square error (RMSE), percentage of retrievals within the expected error (EE), and Global Climate Observing System (GCOS).

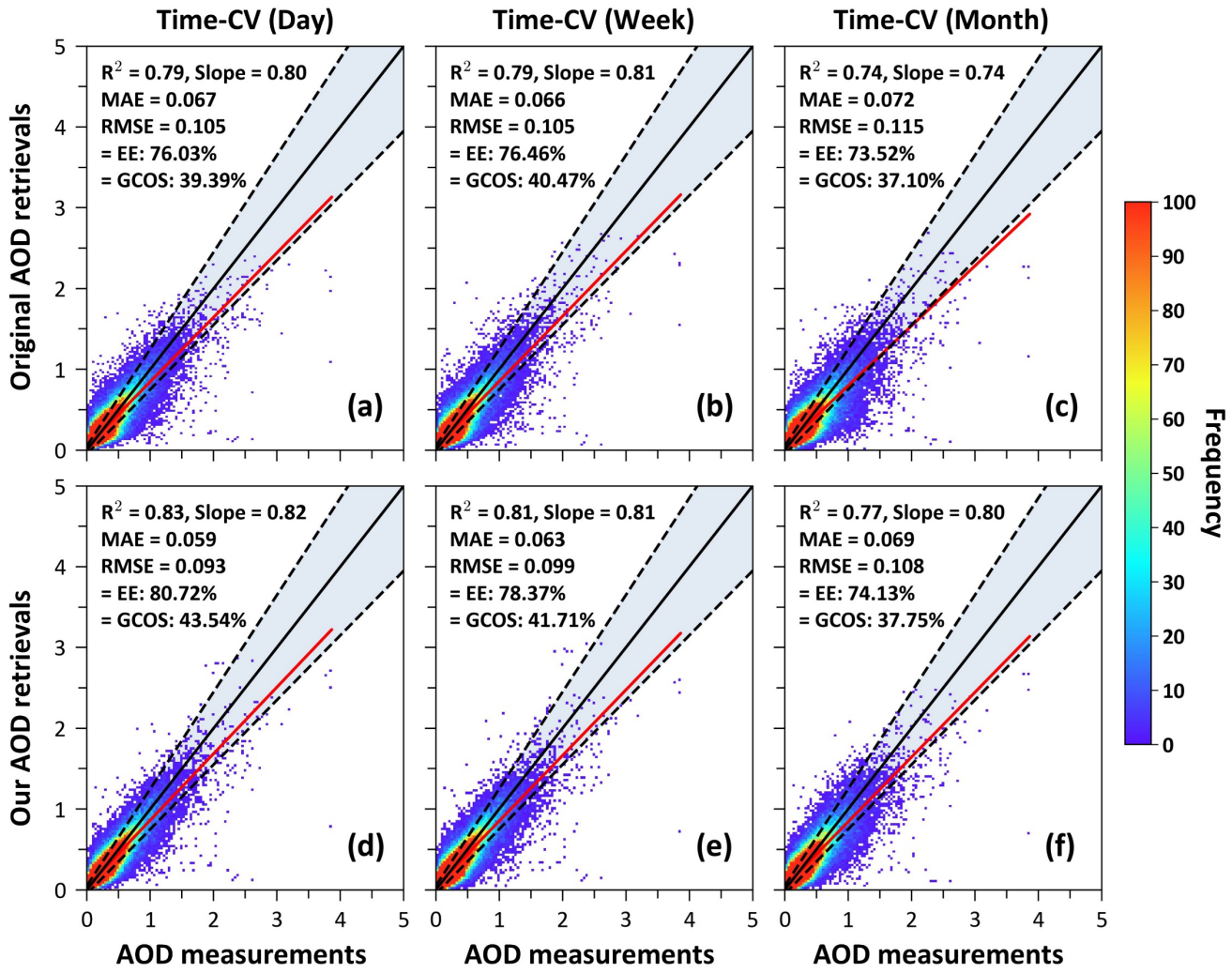

Figure S2. Density scatter plots of (a–c) original models (trained directly without pre-training) and (d–f) our models (pre-trained and fine-tuned) for hourly AOD retrievals against ground-based measurements, assessed using time-based ten-fold cross-validation approaches with increasing temporal intervals (i.e., daily, weekly, and monthly). In each panel, the black dotted line represents the expected error range, the black solid line indicates the 1:1 line, and the red solid line shows the linear regression line. The numbers in the top-left corner of the subfigure represent the coefficient of determination (R^2), slope of the regression line, mean absolute error (MAE), root mean square error (RMSE), percentage of retrievals within the expected error (EE), and Global Climate Observing System (GCOS).

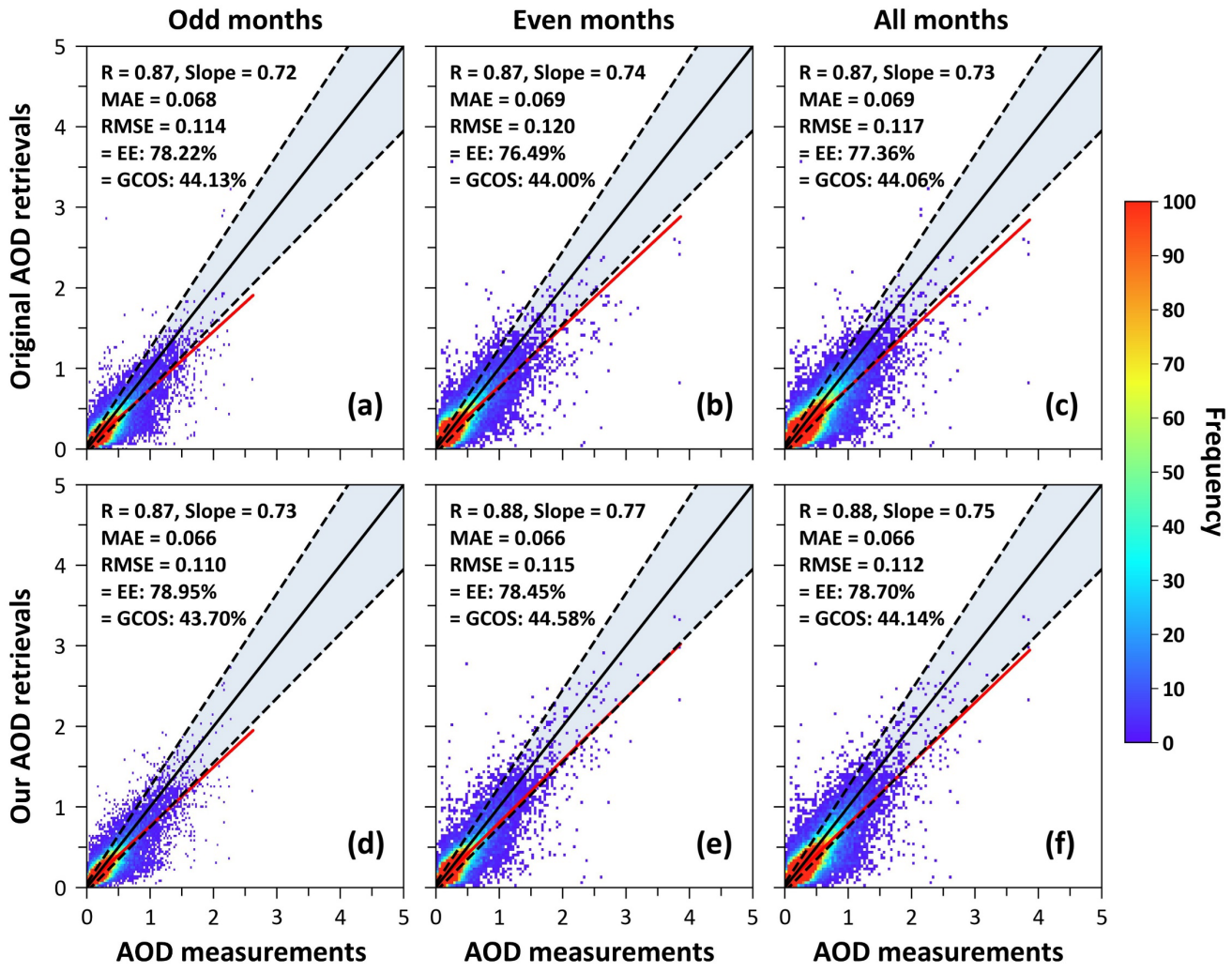

Figure S3. Density scatter plots of (a–c) original models (trained directly without pre-training) and (d–f) our models (pre-trained and fine-tuned) for hourly AOD retrievals against ground-based measurements, with data from each month (i.e., odd months and even months of the year) withheld separately. In each panel, the black dotted line represents the expected error range, the black solid line indicates the 1:1 line, and the red solid line shows the linear regression line. The numbers in the top-left corner of the subfigure represent the correlation coefficient (R), slope of the regression line, mean absolute error (MAE), root mean square error (RMSE), percentage of retrievals within the expected error (EE), and Global Climate Observing System (GCOS).

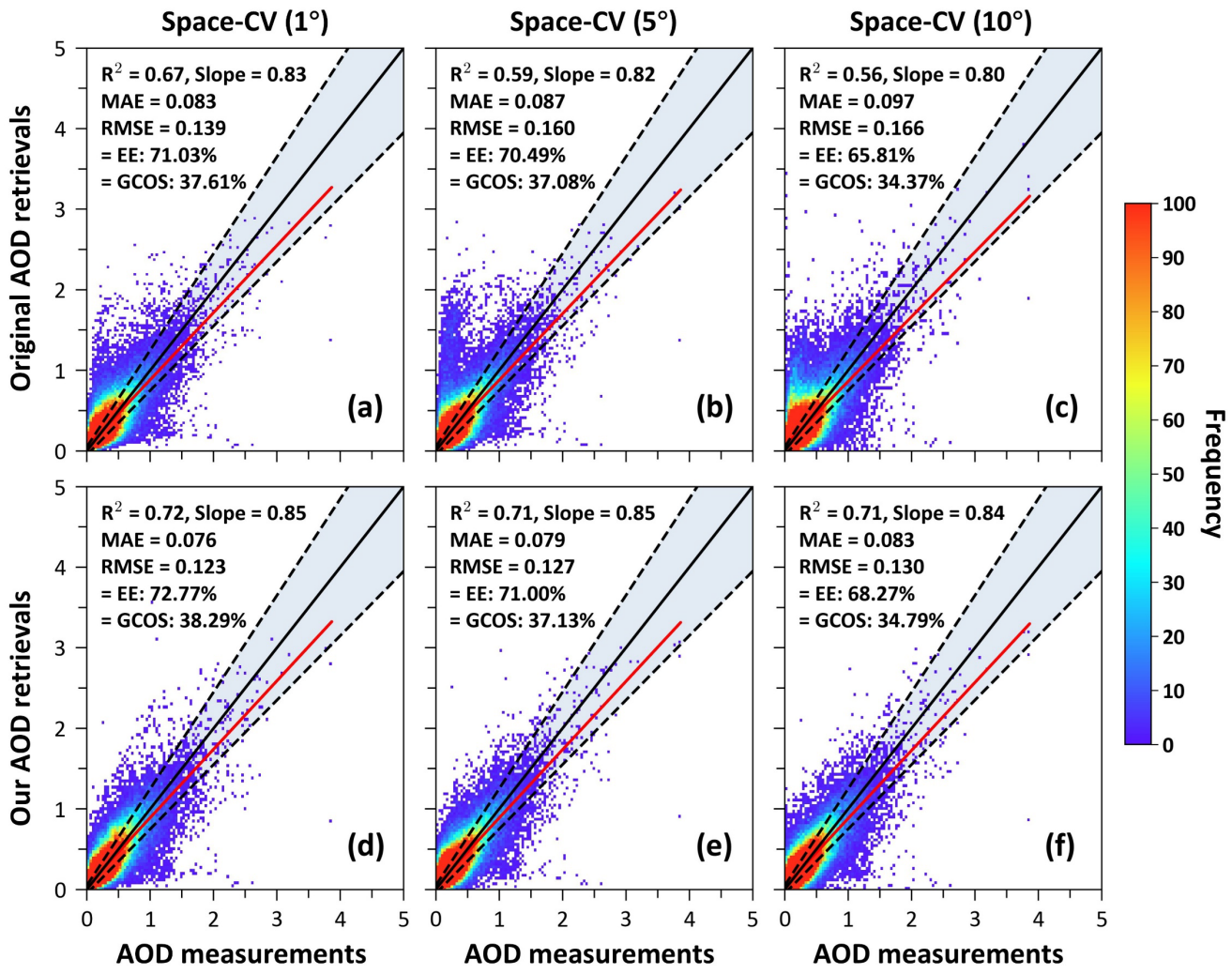

Figure S4. Density scatter plots of (a–c) original models (trained directly without pre-training) and (d–f) our models (pre-trained and fine-tuned) for hourly AOD retrievals against ground-based measurements, assessed using space-based ten-fold cross-validation approaches with increasing spatial intervals (i.e., 1°×1°, 5°×5°, and 10°×10°). In each panel, the black dotted line represents the expected error range, the black solid line indicates the 1:1 line, and the red solid line shows the linear regression line. The numbers in the top-left corner of the subfigure represent the coefficient of determination (R^2), slope of the regression line, mean absolute error (MAE), root mean square error (RMSE), percentage of retrievals within the expected error (EE), and Global Climate Observing System (GCOS).

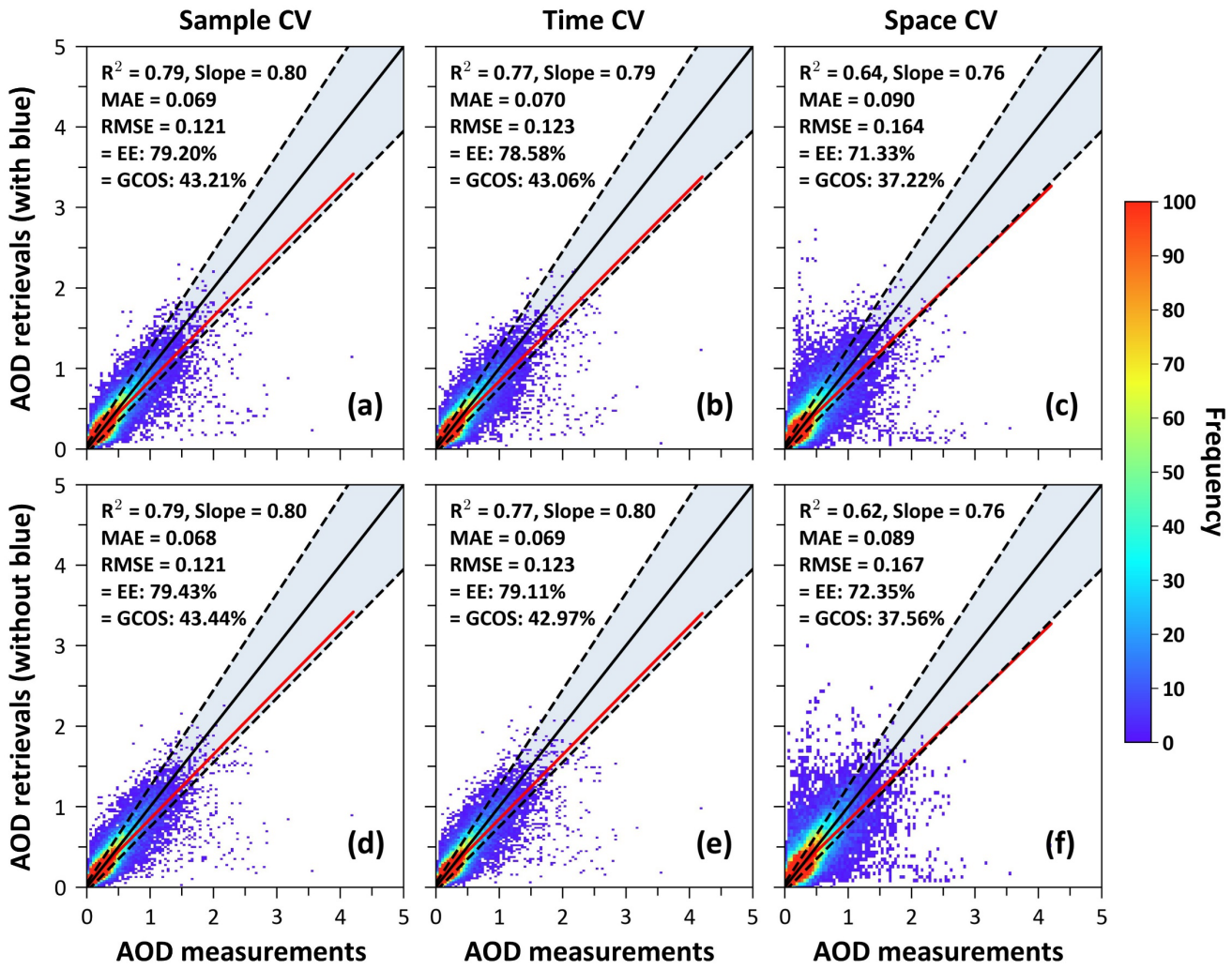

Figure S5. Density scatter plots comparing Himawari-8/AHI hourly AOD retrievals with ground-based measurements using sample-, time-, and space-based ten-fold cross-validation, with (a–c) and without (d–f) the blue band included as inputs to the AeroTrans-Himawari model. In each panel, the black dotted line represents the expected error range, the black solid line indicates the 1:1 line, and the red solid line shows the linear regression line. The numbers in the top-left corner of the subfigure represent the coefficient of determination (R^2), slope of the regression line, mean absolute error (MAE), root mean square error (RMSE), percentage of retrievals within the expected error (EE), and Global Climate Observing System (GCOS).

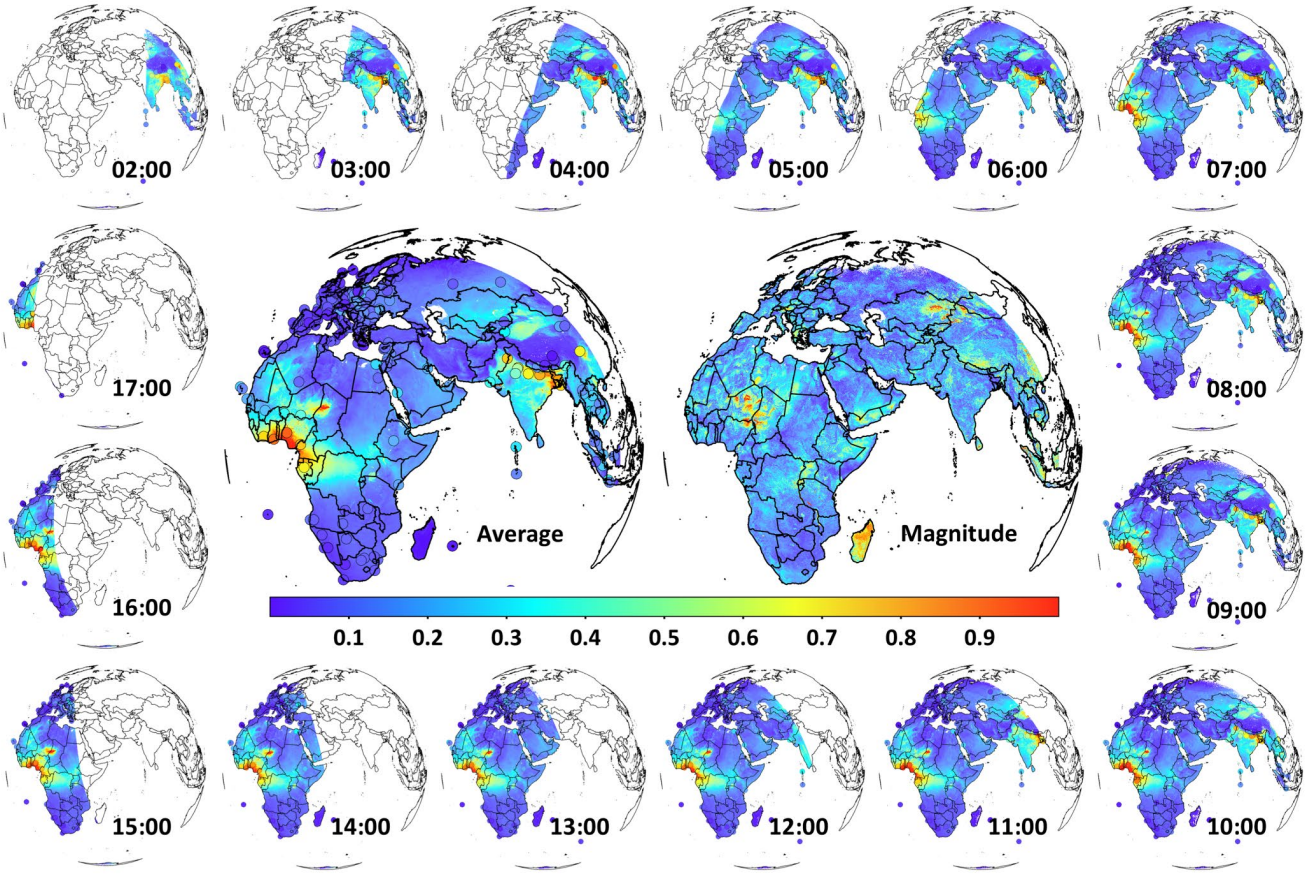

Figure S6. Diurnal variations in AOD at 3-km spatial resolution from 02:00 to 17:00 UTC over Europe, Africa, and West Asia, together with maps of the daily mean AOD and the amplitude of diurnal variation for the Northern Hemisphere winter (December–February).

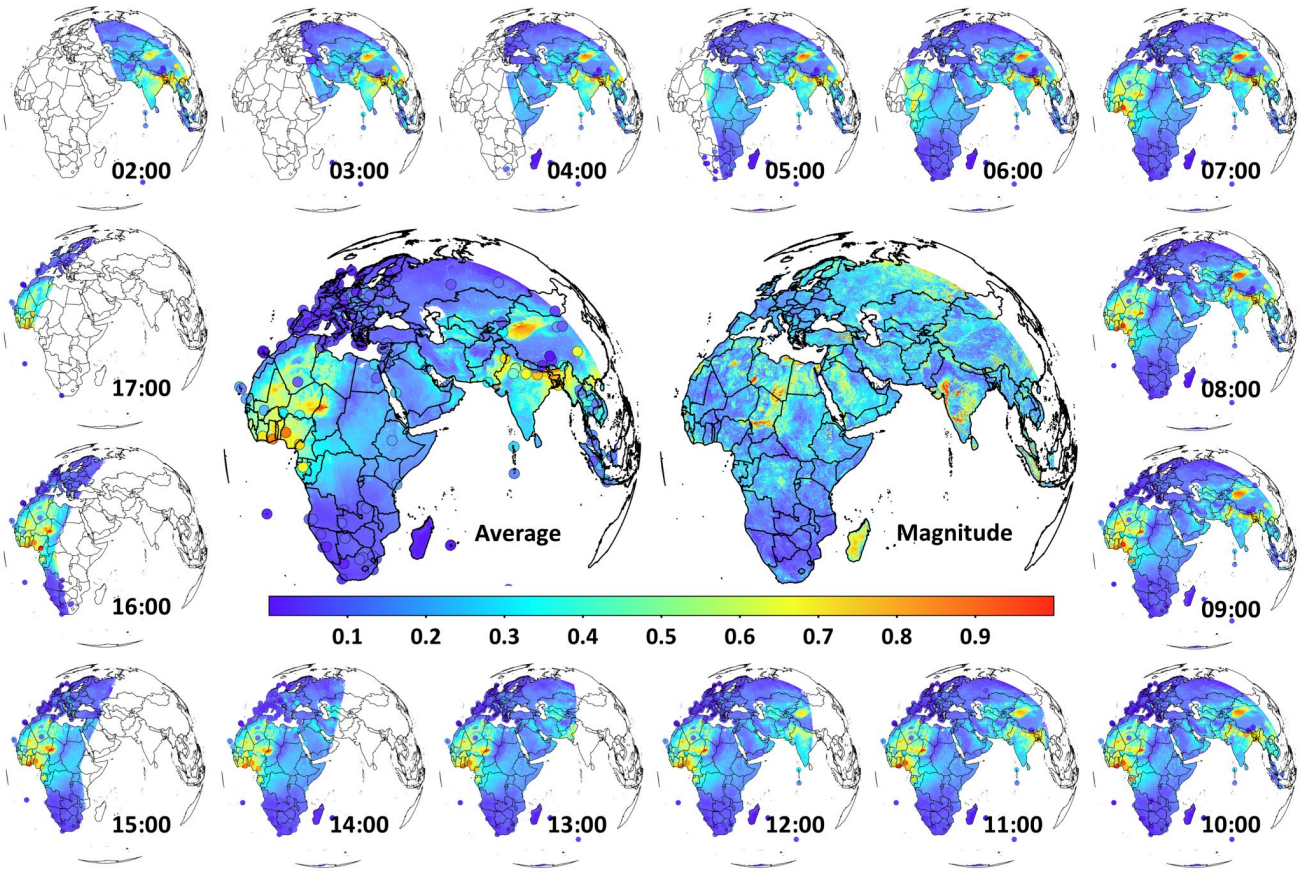

Figure S7. Diurnal variations in AOD at 3-km spatial resolution from 02:00 to 17:00 UTC over Europe, Africa, and West Asia, together with maps of the daily mean AOD and the amplitude of diurnal variation for the Northern Hemisphere spring (March–May).

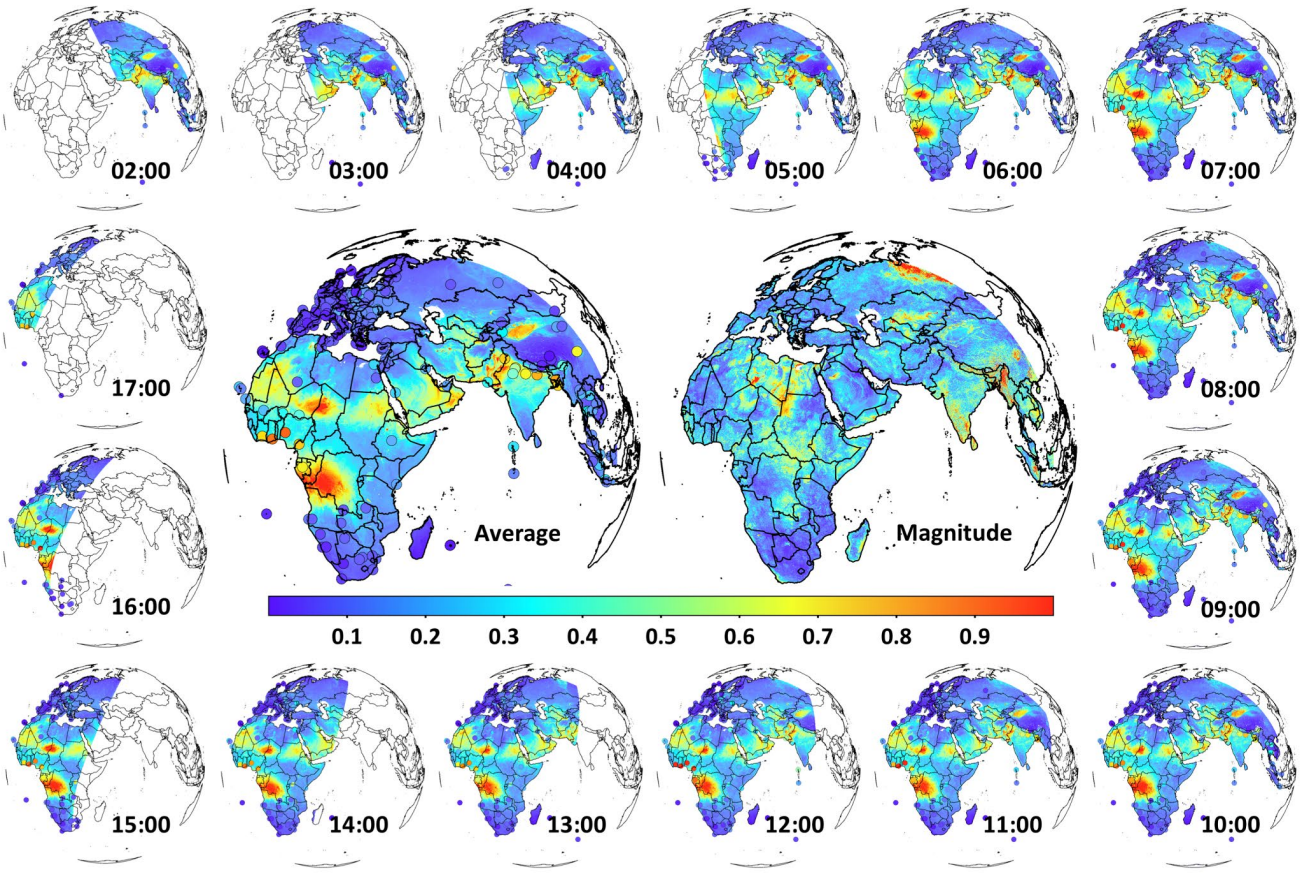

Figure S8. Diurnal variations in AOD at 3-km spatial resolution from 02:00 to 17:00 UTC over Europe, Africa, and West Asia, together with maps of the daily mean AOD and the amplitude of diurnal variation for the Northern Hemisphere summer (June–August).

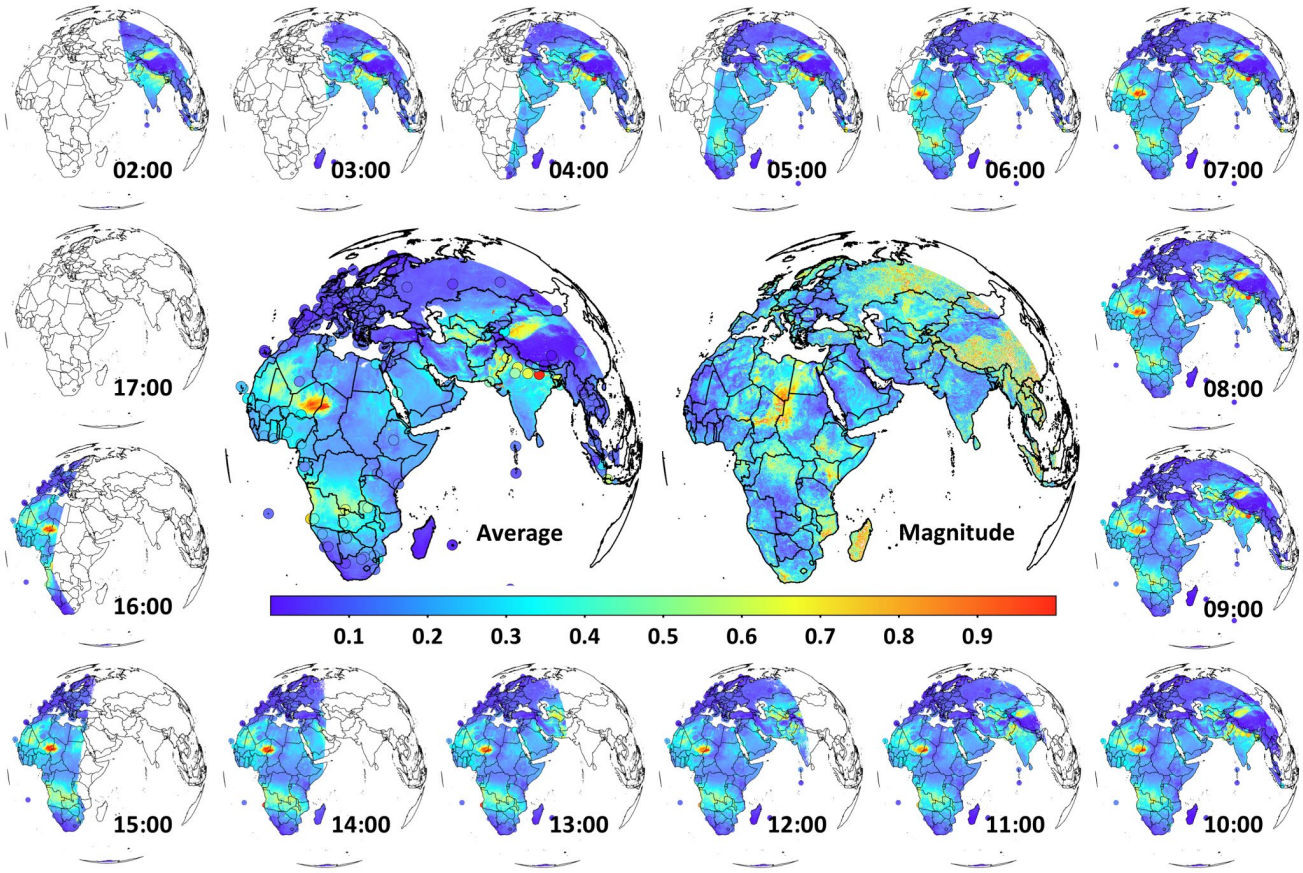

Figure S9. Diurnal variations in AOD at 3-km spatial resolution from 02:00 to 17:00 UTC over Europe, Africa, and West Asia, together with maps of the daily mean AOD and the amplitude of diurnal variation for the Northern Hemisphere autumn (September–November).

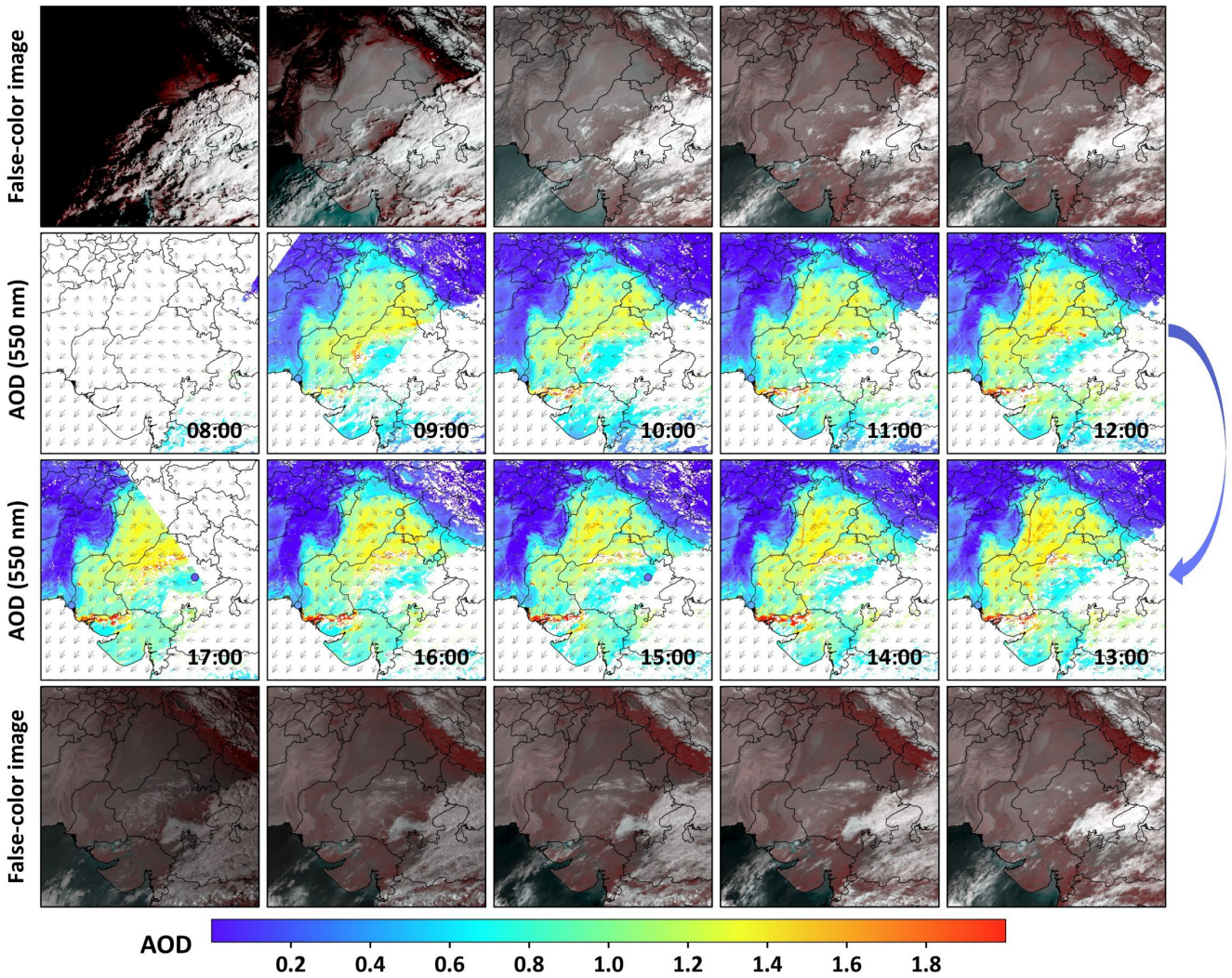

Figure S10. Diurnal distribution and variation of AOD from 08:00–17:00 local time (UTC + 5:00) in Pakistan (65°E–80°E and 20–35°N) during a severe urban haze event on November 20, 2021. Colored dots represent ground-based AOD measurements, and arrows indicate 10 m wind direction from the ERA5-Land reanalysis.

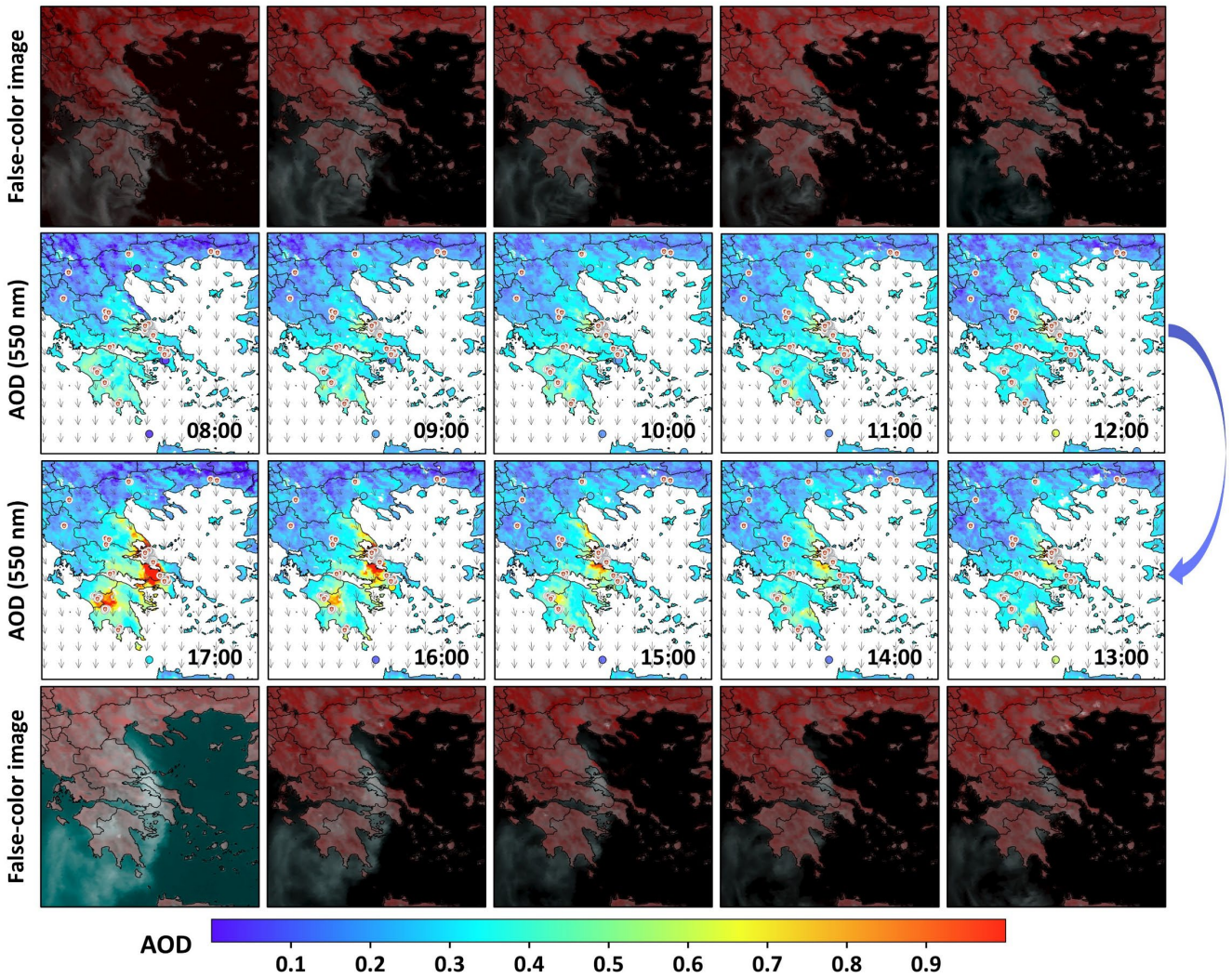

Figure S11. Diurnal distribution and variation of AOD from 08:00–17:00 local time (UTC + 2:00) in Greece (20°E–25°E and 35°N–45°N) during a typical wildfire event on August 8, 2021. Red points denote daily active fire detections from the MCD14A1 product. Colored dots represent ground-based AOD measurements, and arrows indicate 10 m wind direction from the ERA5-Land reanalysis.

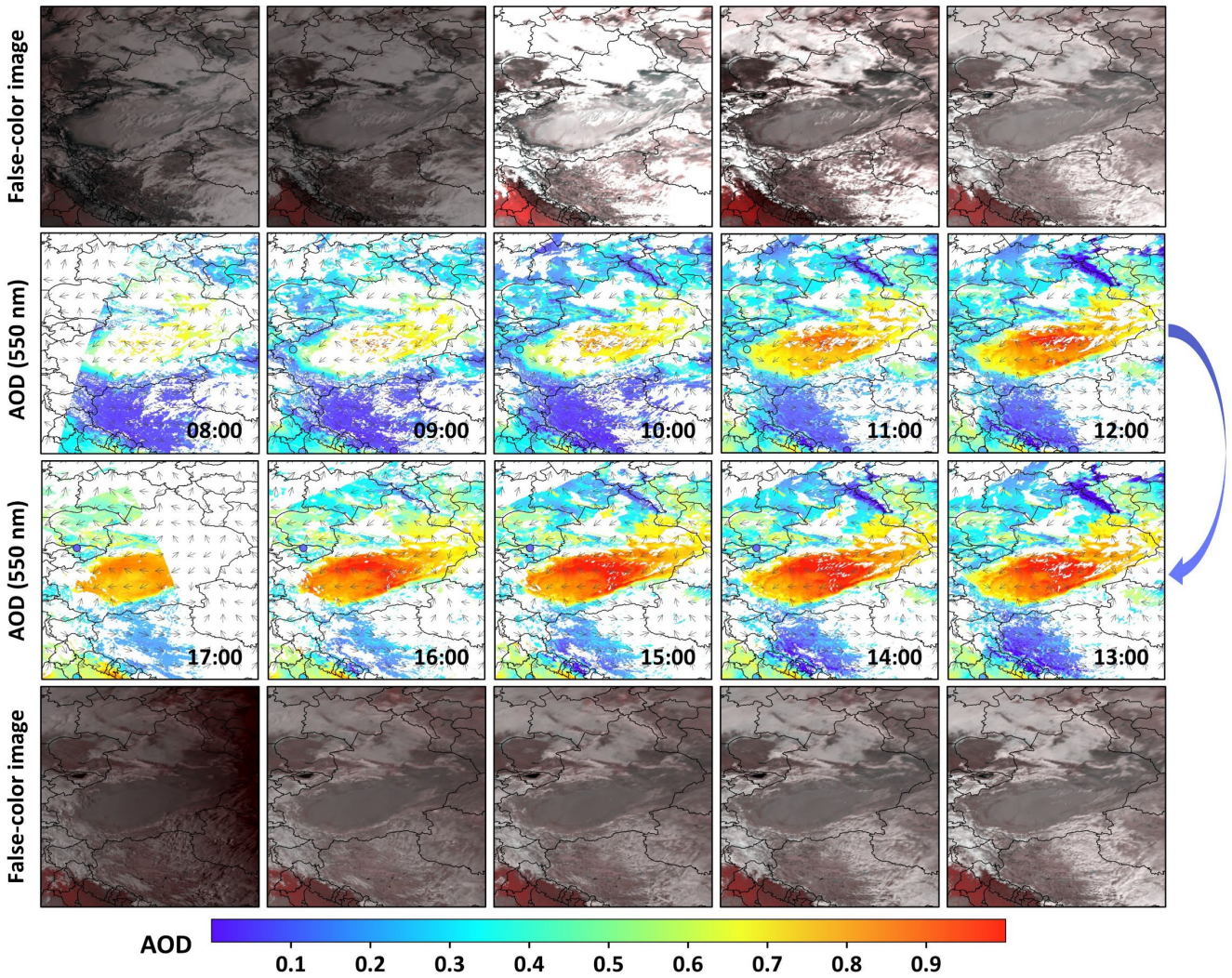

Figure S12. Diurnal distribution and variation of AOD from 08:00–17:00 local time (UTC + 5:00) in the Taklimakan desert (75°E–90°E and 35°N–45°N) during a typical dust storm event on March 6, 2021. Colored dots represent ground-based AOD measurements, and arrows indicate 10 m wind direction from the ERA5-Land reanalysis.

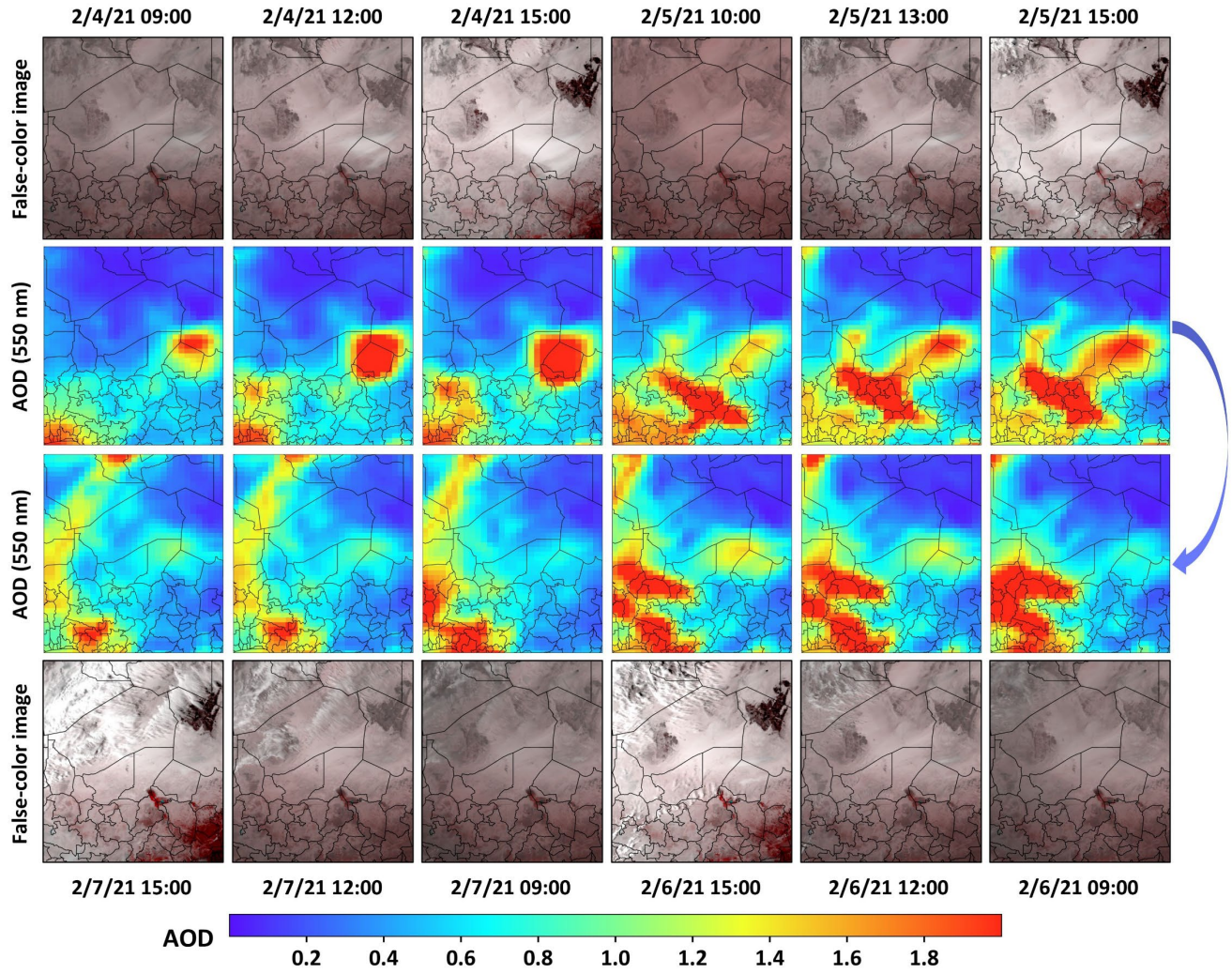

Figure S13. Diurnal distribution and variation of MERRA-2 AOD over the Sahara Desert (5°E–20°E and 10°N–25°N) during a typical dust storm event from 4 to February 9, 2021. Colored dots represent ground-based AOD measurements, and arrows indicate 10 m wind direction from the ERA5-Land reanalysis.

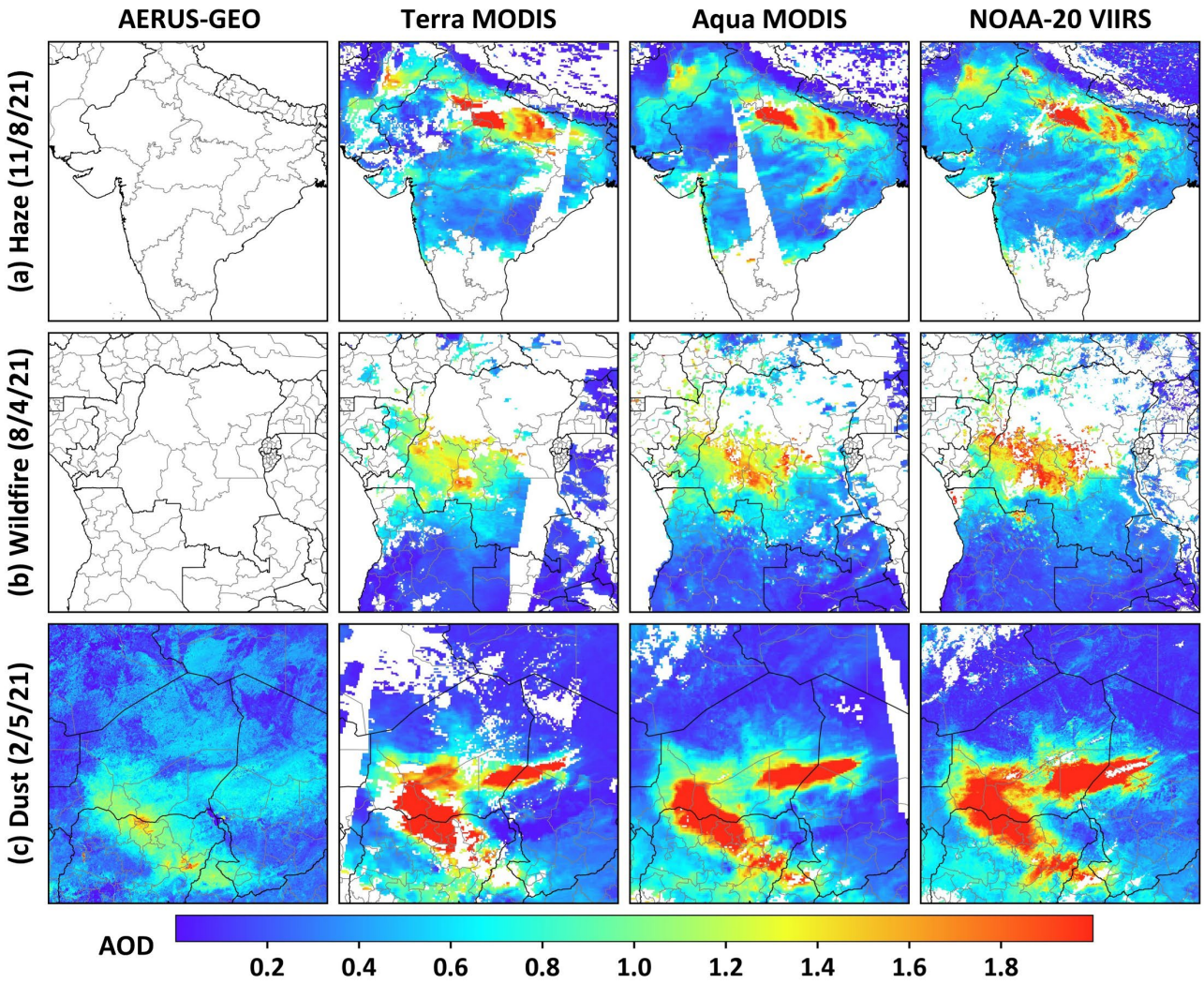

Figure S14. Spatial distributions of available AOD retrievals from MSG-4/SEVIRI AERUS-GEO (635 nm, 3 km, daily-average), Terra/MODIS DB (550 nm, 10 km, ~10:30 local time, LT), Aqua/MODIS DB (550 nm, 10 km, ~13:30 LT), NOAA-20/VIIRS DB (550 nm, 6 km, ~13:30 LT) products during (a) a haze event on November 8, 2021 over India (67°E–89°E, 11°N–33°N), (b) a wildfire event on August 4, 2021 in central and western Africa (10°E–35°E, 17°S–8°N), and (c) a dust storm event on February 5, 2021 in the Sahara Desert (2°E–22°E, 7°N–24°N). The absence of MSG-4 results in (a) and (b) is due to a lack of retrievals during the study period.

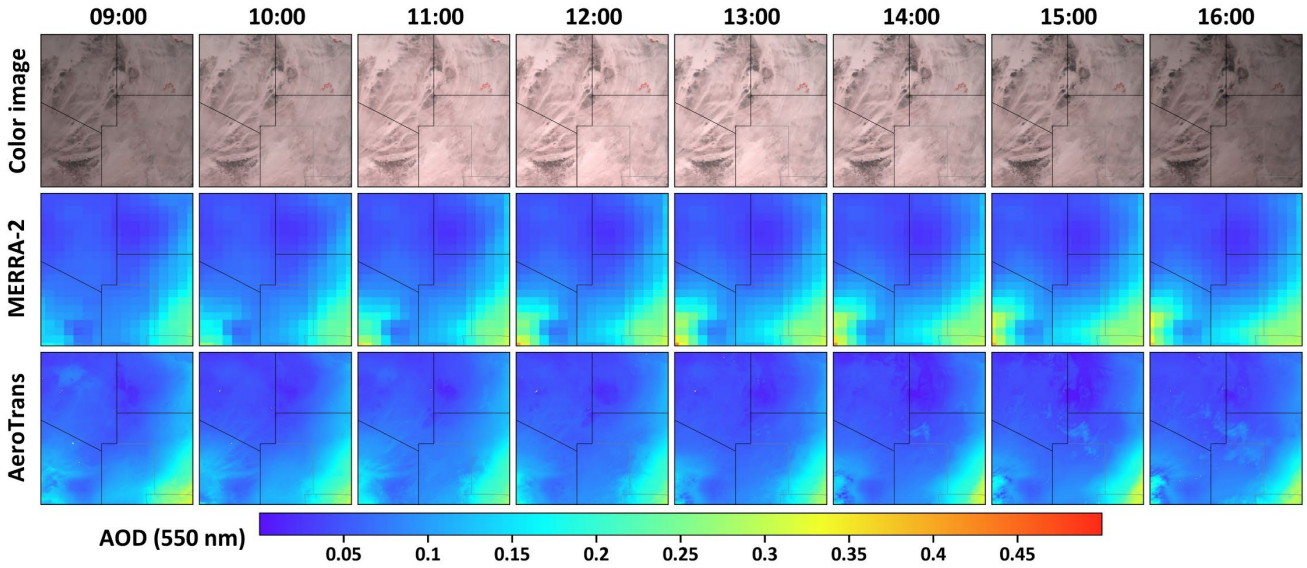

Figure S15. Spatial distributions of hourly AOD over northwestern Africa (20°E–30°E, 16°N–26°N) on February 26, 2021, derived from the MERRA-2 reanalysis and our AeroTrans-MSG model, in a region without available ground-based measurements.

Table S1. Summary of spectral band parameters for the MSG/SEVIRI multispectral instrument.

Band name	Spectral range (μm)	Center wavelength (μm)	Spatial resolution (km)
HRV	0.40–1.10	0.75	1
VIS0.6*	0.56–0.71	0.64	3
VIS0.8*	0.74–0.88	0.81	3
NIR1.6*	1.50–1.78	1.64	3
IR3.9*	3.48–4.36	3.92	3
WV6.2	5.35–7.15	6.25	3
WV7.3	6.85–7.85	7.35	3
IR8.7	8.30–9.10	8.70	3
IR9.7	9.38–9.94	9.66	3
IR10.8	9.80–11.80	10.80	3
IR12.0	11.00–13.00	12.00	3
IR13.4	12.40–14.40	13.40	3

* Indicates bands adopted in this study for AOD retrieval using deep learning

Table S2. Hyperparameter settings for our AeroTrans-MSG model.

Classification	Hyperparameters	Values
Model architecture*	Model input/output	22/1
	num_layers	2
	d_model	22
	nhead	1
	layer_norm_eps	1e-5
	feed-forward dimension	128
	dropout	0.01
	activation	ReLU
	device	CUDA
Training parameter	optimizer	Adam
	loss function	MSE
	learning-rate schedule	halved after 100 epochs; batch size
	batch size	1024
	total training epochs	500
	early stopping	patience = 20 with MSE threshold = 0.001

*Note: The Transformer Encoder model is implemented using PyTorch's torch.nn package with other hyperparameters that use the framework defaults unless specified.